Engineering Science and Technology, an International Journal 19 (2016) 1936–1948

HOSTED BY

Contents lists available at ScienceDirect

Engineering Science and Technology, an International Journal

journal homepage: www.elsevier.com/locate/jestch

Full Length Article

Transient free convective flow in an annular porous medium: A semi-analytical approach

Basant K. Jha, Taiwo S. Yusuf *

Department of Mathematics, Ahmadu Bello University, Zaria, Nigeria

ARTICLE INFO

Article history:
Received 22 June 2016
Accepted 28 September 2016
Available online 13 October 2016

Keywords:
Transient
Free convection
Darcy number
Isothermal
Isoflux
Riemann-sum approximation

ABSTRACT

The transient fully developed free-convective flow of viscous incompressible fluid between two concentric vertical cylinders filled with porous material and saturated with the same fluid have been analysed due to isothermal or isoflux heating of the outer surface of inner cylinder. The governing partial differential equations of motion and energy are transformed into ordinary differential equations using Laplace transform technique. The ordinary differential equations are then solved analytically in Laplace domain. The Riemann-sum approximation method is used to invert the Laplace domain into time domain. The solution obtained is validated by comparison with closed form solution obtained for steady states which has been obtained separately. An excellent agreement was found for transient and steady state solution at large value of time. The governing partial differential equations are also solved by implicit finite difference method to verify the present proposed method. The variation of temperature, velocity, skin-frictions and mass flow rate with dimensionless parameter controlling the present physical situation are illustrated graphically and discussed. It is observed that velocity and temperature increases with time and finally attains its steady state status. Furthermore, both velocity as well as temperature of the fluid is higher in case of isothermal heating of the outer surface of the inner cylinder compared with the isoflux heating case when the gap between the cylinder is less or equal to the radius of inner cylinder while reversed trend is observed when the gap between the cylinders is greater than the radius of inner cylinder for all considered values of time.

1. Introduction

Fluid flow as a result of buoyancy force due to temperature difference in a porous medium are found in wide range of application in engineering such as operation of solar collectors, cooling system in electronics equipment, water purification, ground water studies. A good survey of the existing literature shows that flow through a porous medium has been on the increase in recent years. To mention but few, Vafai and Tien [1] presented the importance of Brinkman and Forchheimer terms in forced convection over a flat plate. They obtained the resulting error in heat transfer coefficient when the viscous and inertia terms are neglected. Jha [2] extensively did the analysis of the closed-form solution of natural convection flow through a vertical annular duct filled with porous media for more general thermal boundary condition at the outer surface of the inner cylinder using the non-Darcian flow model derived by Vafai and Tien [1]. Paul and Singh [3] investigated fully developed natural convection flow between coaxial vertical cylinders partially filled with a porous material. In which they observed that the velocity is influenced by the shear stress jump condition at the interface.

In another article, Joshi [4] studied the fully developed free-convection flows in vertical annulus with two isothermal boundaries. In a related work, Singh and Singh [5] considered the effect of induced magnetic field on natural convection flow in vertical concentric annulus. In their work they found that the velocity fields are the same when the outer surface of the inner cylinder is either heated isothermal or constant heat flux when the annular gap is 1.71.

The transient free-convective flow through a vertical porous annulus has been discussed by Jha et al. [6] when the thermal boundary condition is maintained at a constant temperature or at a constant heat flux. They obtained that the steady state temperature and velocity are independent of Prandtl number in the absence of suction/injection. Javaherdeh et al. [7] studied natural

* Corresponding author.
E-mail addresses: basant777@yahoo.co.uk (B.K. Jha), taiyeee@yahoo.com (T.S. Yusuf).

Peer review under responsibility of Karabuk University.

http://dx.doi.org/10.1016/j.jestch.2016.09.022
2215-0986/

Nomenclature

t'	dimensional time
r'	dimensional radial coordinate
U'	axial velocity
U	dimensionless axial velocity
R	dimensionless radial coordinate
T_0	initial temperature ($t' \leqslant 0$)
T_w	temperature of the outer surface of the inner cylinder in the case of isothermal heating ($t' > 0$)
θ	dimensionless temperature
a	radius of the inner cylinder
b	radius of the outer cylinder
g	gravitational acceleration
Q	dimensionless mass flow rate
Pr	Prandtl number
C_p	specific heat at constant pressure
t	dimensionless time
K	permeability of the Porous medium
k	thermal conductivity of the fluid
Da	Darcy number
q'	constant heat flux

Greek letters

υ	kinematic viscosity of fluid
υ_{eff}	effective kinematic viscosity of fluid
τ	skin friction
ρ	density
λ	radius ratio (b/a)
q'	constant heat flux
Γ	ratio of viscosity

convection heat and mass transfer in MHD fluid flow past a moving vertical plate with variable surface temperature and concentration in a porous medium.

In another related work Jha and Odengle [8] did a numerical investigation on unsteady Couette flow in a composite channel partially filled with porous material using a semi- analytical approach. This numerical scheme has been found to be in agreement with the steady state solution and it has been adopted in this research. Recently, Vanita and Kumar [9] examined the effect of radial magnetic field on natural convection flow in alternate conducting vertical concentric annuli with ramped temperature.

In the Recent past, Arpino et al. [10] presented a numerical result of transient thermal analysis of natural convection in porous and partially porous cavities. They applied the stabilized AC–CBS algorithm and are of the opinion that, the AC–CBS algorithm represents a powerful tool for the study of transient natural convection in partly porous tall cavities. Similar numerical analysis was also carried out by Massarotti et al. [11] in partially porous annuli.

Other previous works in porous medium in an annular geometry also reviewed are [12–18].

This work is aimed at providing the semi-analytical solution to the transient free-convective flow in a vertical annulus filled with porous material when thermal boundary condition at the outer surface of inner cylinder is of mixed kind while inner surface of outer cylinder is of first-kind.

2. Mathematical analysis

The geometry of the system under consideration for the present physical situation is shown in Fig. 1. Consider the transient fully developed free-convective flow of viscous, incompressible fluid in a vertical annulus filled with isotropic porous material. A cylindrical co-ordinate system is chosen such that the X'-axis is taken along the axis of the cylinders in the vertical upward direction and r'-axis is in the radial direction. The radii of the inner and outer cylinders are a and b respectively. At time $t' \leqslant 0$, both fluid and cylinders are assumed to be at temperature T_0. At time $t' > 0$, the temperature of the outer surface of the inner cylinder is raised to T_w ($T_w > T_0$) or heat is supplied at constant rate q' while the inner surface of the outer cylinder is maintained at T_0, causing the transient free-convection current. Since the flow is fully developed and the cylinders are of infinite length, the flow depends only on radial co-ordinate (r') and time (t'). Under the usual Boussinesq approximation, the mathematical model representing the present physical situation in dimensional form are:

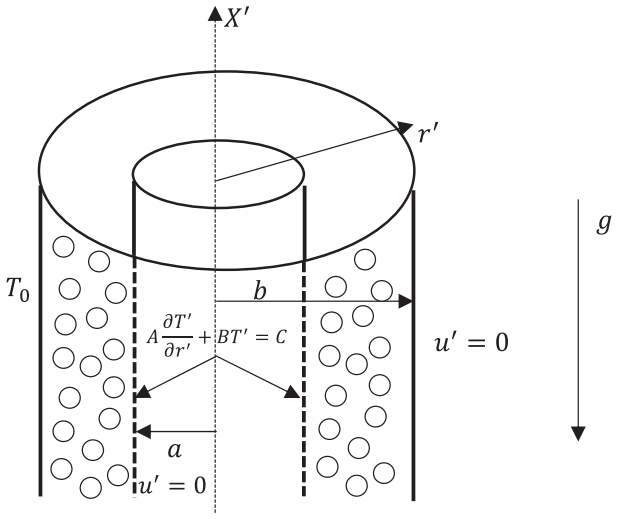

Fig. 1. Schematic diagram of the problem.

$$\frac{\partial U'}{\partial t'} = \upsilon_{eff}\left[\frac{\partial^2 U'}{\partial r'^2} + \frac{1}{r'}\frac{\partial U'}{\partial r'}\right] + g\beta(T' - T_0) - \frac{\upsilon}{K}U' \tag{1}$$

$$\frac{\partial T'}{\partial t'} = \frac{k}{\rho c_p}\left[\frac{\partial^2 T'}{\partial r'^2} + \frac{1}{r'}\frac{\partial T'}{\partial r'}\right] \tag{2}$$

The initial and boundary condition relevant to the present problem under consideration are

$$\begin{aligned} &t' \leqslant 0 \quad U' = 0,\ T' = T_0 \quad a \leqslant r' \leqslant b \\ &t' > 0 \quad \begin{cases} U' = 0 & \frac{\partial T'}{\partial r'} = -\frac{q'}{k} \text{ or } T' = T_w \text{ at } r' = a \\ U' = 0 & T' = T_0 \text{ at } r' = b \end{cases} \end{aligned} \tag{3}$$

Introducing the following non-dimensional quantities:

$$\begin{aligned} &t = \frac{t'\upsilon}{a^2}, R = \frac{r'}{a}, \lambda = \frac{b}{a}, Da = \frac{K}{a^2}, \theta = \frac{(T' - T_0)}{\Delta T}, \\ &Pr = \frac{\boldsymbol{\mu c_p}}{\mathbf{k}}, U = \frac{U'}{U_0}, U_0 = \frac{g\beta a^2 \Delta T}{\upsilon} \end{aligned} \tag{4}$$

where $\Delta T = T_w - T_0$ or $\frac{q'a}{k}$ according as inner cylinder is maintained at constant temperature T_w or constant heat flux q', respectively. Using Eq. (4), the dimensionless momentum and energy equations are

Table 1
Numerical values of the steady-state velocity obtained using the Riemann-sum approximation approach, implicit finite difference method and the exact solution given in Jha [2] ($Pr = 0.71,\ \Gamma = 1,\ \lambda = 2.0$).

		Isothermal case			Constant heat flux case		
R	Da	Riemann-sum approximation	Implicit finite difference	Exact solution [2]	Riemann-sum approximation	Implicit finite difference	Exact solution [2]
1.2	0.1	0.0252	0.0252	0.0252	0.0174	0.0174	0.0174
	0.01	0.0061	0.0061	0.0061	0.0042	0.0042	0.0043
1.4	0.1	0.0279	0.0279	0.0279	0.0193	0.0193	0.0193
	0.01	0.0050	0.0050	0.0050	0.0035	0.0034	0.0035
1.6	0.1	0.0211	0.0211	0.0211	0.0147	0.0147	0.0147
	0.01	0.0032	0.0032	0.0032	0.0022	0.0022	0.0022
1.8	0.1	0.0109	0.0109	0.0109	0.0075	0.0075	0.0075
	0.01	0.0015	0.0015	0.0015	0.0010	0.0010	0.0011

Table 2
Numerical values of the transient state velocity obtained using the Riemann-sum approximation method, implicit finite difference and that obtained from the exact solution Jha [2] when ($R = 1.6,\ \Gamma = 1$ and $\lambda = 2.0$).

		Isothermal case			Constant heat flux case		
Da	t	Riemann-sum approximation	Implicit finite difference	Exact solution [2]	Riemann-sum approximation	Implicit finite difference	Exact solution [2]
0.01	0.08	0.0015	0.0015	0.0032	0.0003	0.0003	0.0022
	0.10	0.0019	0.0019	0.0032	0.0004	0.0004	0.0022
	0.20	0.0029	0.0029	0.0032	0.0011	0.0010	0.0022
	3.00	0.0032	0.0032	0.0032	0.0022	0.0022	0.0022
	4.00	0.0032	0.0032	0.0032	0.0022	0.0022	0.0022
0.1	0.08	0.0061	0.0061	0.0211	0.0011	0.0011	0.0147
	0.10	0.0086	0.0086	0.0211	0.0018	0.0016	0.0147
	0.20	0.0171	0.0170	0.0211	0.0059	0.0054	0.0147
	3.00	0.0211	0.0211	0.0211	0.0147	0.0147	0.0147
	4.00	0.0211	0.0211	0.0211	0.0147	0.0147	0.0147

Table 3
Numerical values of the steady-state skin-frictions for isothermal and constant heat flux cases given in [2] for different values of *Da* and λ.

λ	Da	Isothermal case		Constant heat flux case	
		τ_1	τ_λ	τ_1	τ_λ
1.6	0.1	0.1652	0.0556	0.0776	0.0261
	0.01	0.0836	0.0129	0.0393	0.0060
1.8	0.1	0.1971	0.0563	0.1158	0.0331
	0.01	0.0878	0.0094	0.0516	0.0055
3.0	0.1	0.2721	0.0296	0.2989	0.0326
	0.01	0.0957	0.0030	0.1052	0.0033
4.0	0.1	0.2910	0.0180	0.4034	0.0249
	0.01	0.0976	0.0018	0.1354	0.0025

Table 4
Numerical values of the steady-state skin-frictions for isothermal and constant heat flux cases using implicit finite difference method for different values of *Da* and λ.

λ	Da	Isothermal case		Constant heat flux case	
		τ_1	τ_λ	τ_1	τ_λ
1.6	0.1	0.1650	0.0557	0.0775	0.0262
	0.01	0.0830	0.0129	0.0390	0.0061
1.8	0.1	0.1967	0.0563	0.1156	0.0331
	0.01	0.0869	0.0094	0.0511	0.0055
3.0	0.1	0.2695	0.0297	0.2943	0.0323
	0.01	0.0906	0.0030	0.0991	0.0033
4.0	0.1	0.2851	0.0179	0.3653	0.0215
	0.01	0.0876	0.0018	0.1133	0.0022

Table 5
Numerical values of the steady state skin-frictions for isothermal and constant heat flux cases using Riemann-sum approximation approach for different values of *Da* and λ.

λ	Da	Isothermal case		Constant heat flux case	
		τ_1	τ_λ	τ_1	τ_λ
1.6	0.1	0.1655	0.0557	0.0777	0.0262
	0.01	0.0838	0.0129	0.0393	0.0061
1.8	0.1	0.1974	0.0563	0.1159	0.0331
	0.01	0.0881	0.0094	0.0517	0.0055
3.0	0.1	0.2724	0.0297	0.2975	0.0323
	0.01	0.0960	0.0030	0.1048	0.0033
4.0	0.1	0.2911	0.0179	0.3774	0.0219
	0.01	0.0979	0.0018	0.1278	0.0022

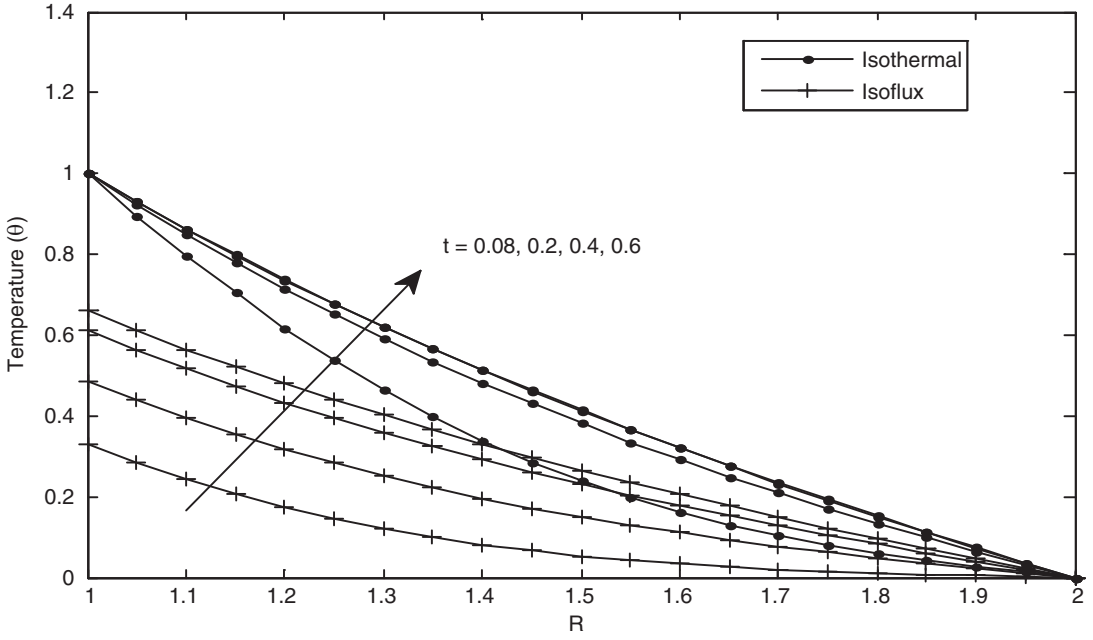

Fig. 2. Temperature variation for different values of time (t) ($Pr = 0.71, \lambda = 2.0$).

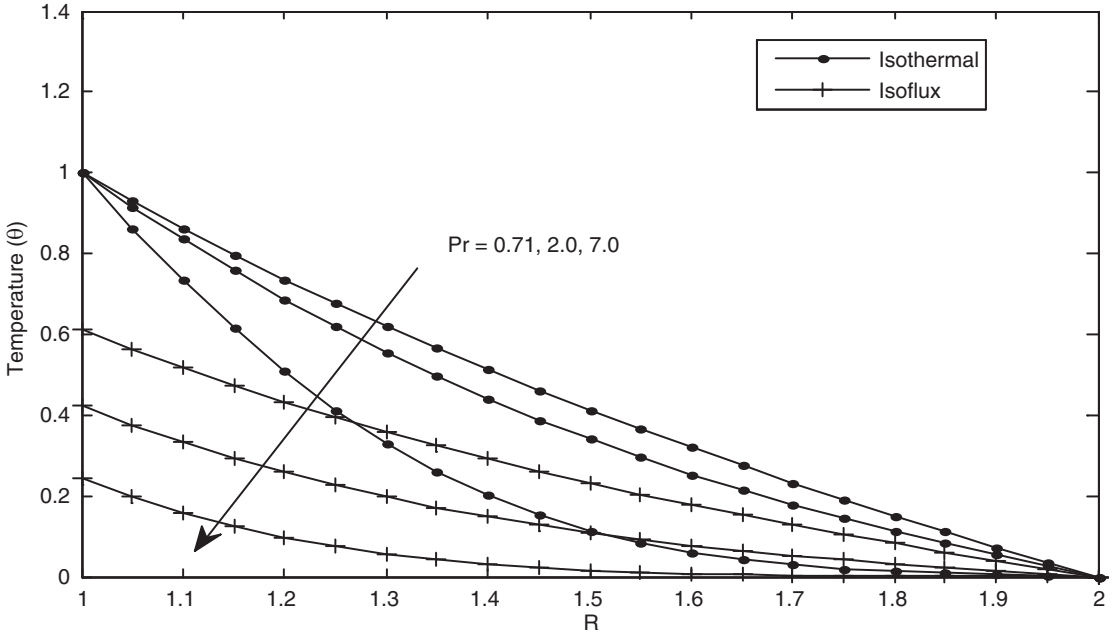

Fig. 3. Temperature variation for different values of Pr($t = 0.4, \lambda = 2.0$).

$$\frac{\partial U}{\partial t} = \Gamma\left[\frac{\partial^2 U}{\partial R^2} + \frac{1}{R}\frac{\partial U}{\partial R}\right] - \frac{U}{Da} + \theta \tag{5}$$

$$\frac{\partial \theta}{\partial t} = \frac{1}{Pr}\left[\frac{\partial^2 \theta}{\partial R^2} + \frac{1}{R}\frac{\partial \theta}{\partial R}\right] \tag{6}$$

The initial and boundary condition in dimensionless form are

$$t \leqslant 0 \quad U = 0,\ \theta = 0 \quad 1 \leqslant R \leqslant \lambda$$
$$t > 0 \quad \begin{cases} U = 0 & \frac{\partial \theta}{\partial R} = -1 \text{ or } \theta = 1 \text{ at } R = 1 \\ U = 0 & \theta = 0 \text{ at } R = \lambda \end{cases} \tag{7}$$

Taking the Laplace transform of Eqs. (5) and (6) we have the following ordinary differential equations

$$\frac{d^2\bar{U}}{dR^2} + \frac{1}{R}\frac{d\bar{U}}{dR} - \frac{1}{\Gamma}\left(\frac{1}{\mathrm{Da}} + s\right)\bar{U} + \frac{\bar{\theta}}{\Gamma} = 0 \tag{8}$$

$$\frac{d^2\bar{\theta}}{dR^2} + \frac{1}{R}\frac{d\bar{\theta}}{dR} - sPr\bar{\theta} = 0 \tag{9}$$

where

$$\bar{U}(R,s) = \int_0^\infty U(R,t)e^{-st}dt,\ \bar{\theta}(R,s) = \int_0^\infty \theta(R,t)e^{-st}dt$$

and $s > 0$.

The Laplace transformation of the boundary conditions are

$$\bar{U} = 0 \quad \frac{d\bar{\theta}}{dR} = -\frac{1}{s} \text{ or } \bar{\theta} = \frac{1}{s} \text{ at } R = 1 \tag{10}$$

$$\bar{U} = 0 \quad \bar{\theta} = 0 \quad \text{at } R = \lambda \tag{11}$$

A unified solution for both the cases (isothermal and isoflux heating) can be obtained by combining the conditions for the temperature at the outer surface of the inner cylinder. By doing so, a combined boundary condition of mixed kind in Laplace domain can be written as

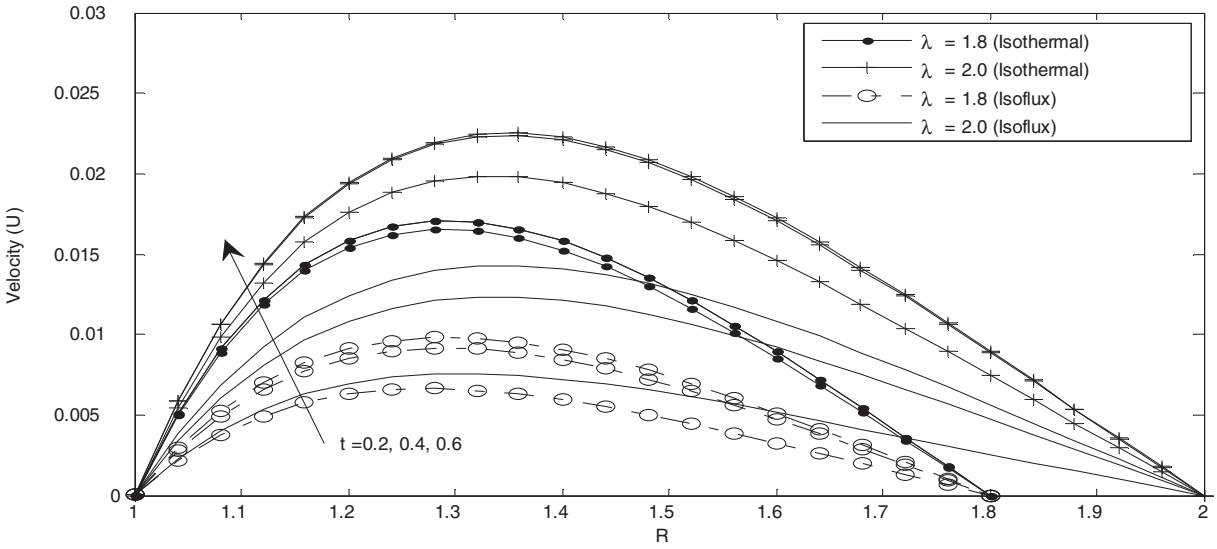

Fig. 4. Velocity variation for different values time (t) ($\mathrm{Da} = 0.1, Pr = 0.71, \Gamma = 1.5, \lambda = 1.8 \& \lambda = 2.0$).

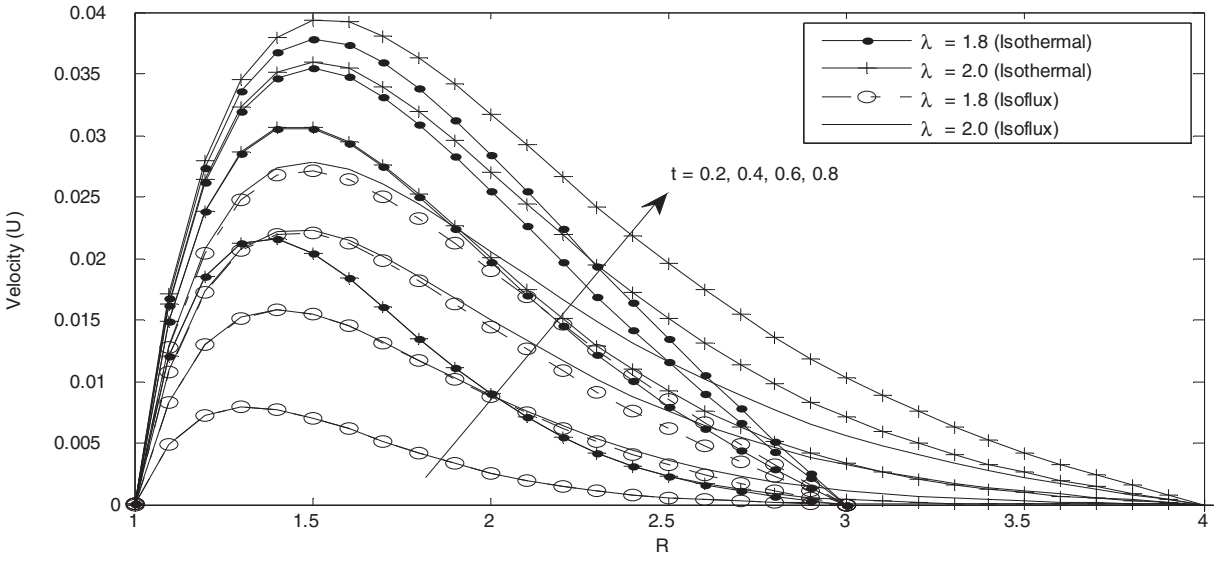

Fig. 5. Velocity variation for different values of time (t) ($\mathrm{Da} = 0.1, Pr = 0.71, \Gamma = 1.5, \lambda = 3 \& \lambda = 4.0$).

$$A\frac{d\bar{\theta}(1)}{dR}+B\bar{\theta}(1)=\frac{C}{s} \tag{12}$$

In which the suitable values of A, B and C give the desired case.

The solutions of Eqs. (8) and (9) in Laplace domain subject to the boundary conditions (11) and (12) are

$$\bar{\theta}(R,s)=C_1I_0(R\sqrt{sPr})+C_2K_0(R\sqrt{sPr}) \tag{13}$$

$$\bar{U}(R,s)=C_3I_0(R\delta)+C_4K_0(R\delta) - \frac{[C_1I_0(R\sqrt{sPr})+C_2K_0(R\sqrt{sPr})]}{\left[\Gamma sPr-\left(\frac{1}{Da}+s\right)\right]} \tag{14}$$

where $\delta=\left[\frac{1}{\Gamma}\left(\frac{1}{Da}+s\right)\right]^{1/2}$

Eq. (13) is to be inverted in order to obtain the temperature solution in time domain. Due to the complex nature of this inversion, we adopt a numerical procedure used in Jha and Odengle [8] which is based on the Riemann-sum approximation. According to this procedure, any function in the Laplace domain can be inverted to the time domain as follows.

$$\theta(R,t)=\frac{e^{\varepsilon t}}{t}\left[\frac{1}{2}\bar{\theta}(R,\varepsilon)+Re\sum_{n=1}^{M}\bar{\theta}\left(R,\varepsilon+\frac{in\pi}{t}\right)(-1)^n\right] \tag{15}$$

where Re refers to the real part of, $i=\sqrt{-1}$, the imaginary number, M is the number of terms used in the Riemann-sum approximation and ε is the real part of the Bromwich contour that is used in inverting Laplace transforms. The Riemann-sum approximation for the Laplace inversion involves a single summation for the numerical process its accuracy depends on the value of ε and the truncation error dictated by M. According to Tzou [19], the value of εt that best satisfied the result is 4.7.

2.1. Skin friction and mass flow rate

The skin frictions at $R=1$ is $\bar{\tau}_1(1,s)$ and $R=\lambda$ is $\bar{\tau}_\lambda(\lambda,s)$ in Laplace domain are obtained by differentiating Eq. (14). Similarly, the mass flow rate of the fluid through the annulus in Laplace domain $\bar{Q}(R,s)$, is obtained by evaluating the integral $2\pi\int_1^\lambda R\bar{U}(R,s)dR$. The solutions are as follows:

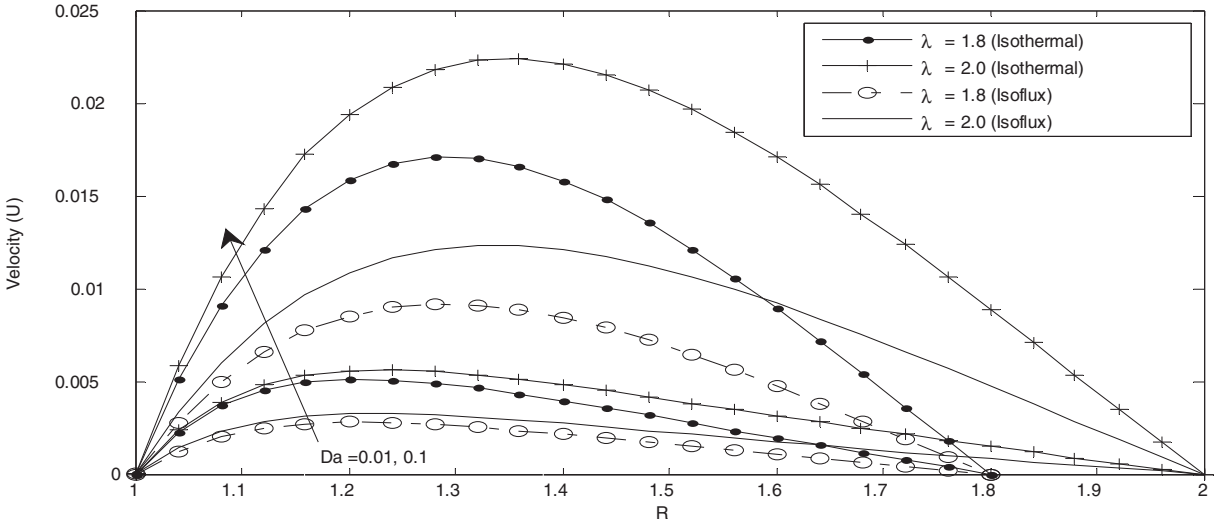

Fig. 6. Velocity variation for different values of Da ($\Gamma=1.5, Pr=0.71, t=0.4, \lambda=1.8\&\lambda=2.0$).

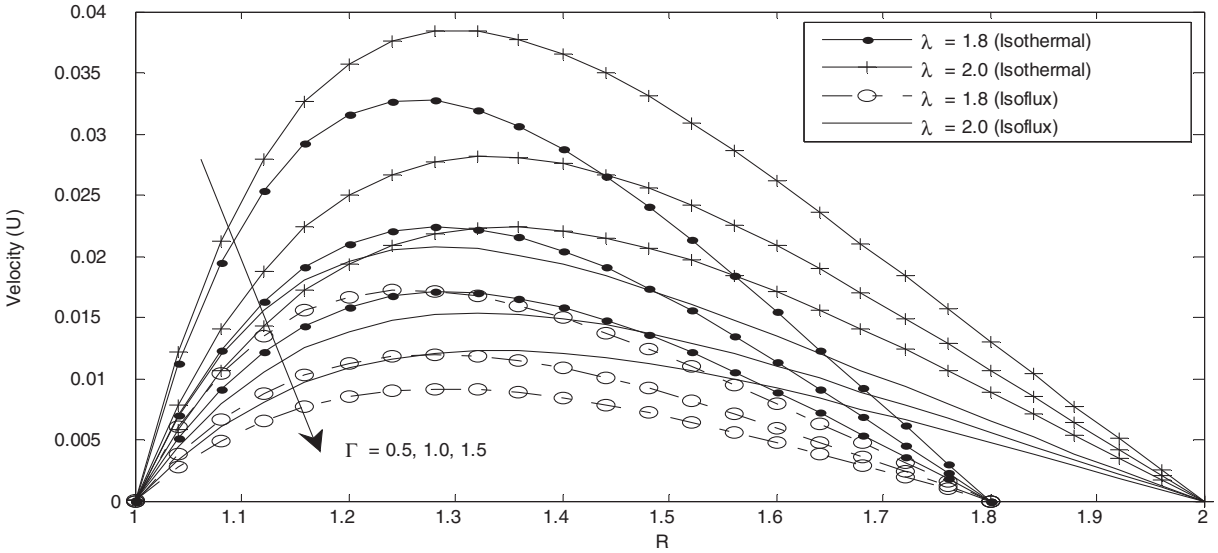

Fig. 7. Velocity variation for different values $\Gamma(\mathrm{Da}=0.1, Pr=0.71, t=0.4, \lambda=1.8\&\lambda=2.0)$.

$$\bar{\tau}_1 = \left.\frac{d\bar{U}}{dR}\right|_{R=1} = \delta[C_3 I_1(\delta) - C_4 K_1(\delta)] - \frac{\sqrt{sPr}[C_1 I_1(\sqrt{sPr}) - C_2 K_1(\sqrt{sPr})]}{\left[\Gamma sPr - \left(\frac{1}{Da} + s\right)\right]} \quad (16)$$

$$\bar{\tau}_\lambda = -\left.\frac{d\bar{U}}{dR}\right|_{R=\lambda} = \delta[C_4 K_1(\lambda\delta) - C_3 I_1(\lambda\delta)] + \frac{\sqrt{sPr}[C_1 I_1(\lambda\sqrt{sPr}) - C_2 K_1(\lambda\sqrt{sPr})]}{\left[\Gamma sPr - \left(\frac{1}{Da} + s\right)\right]} \quad (17)$$

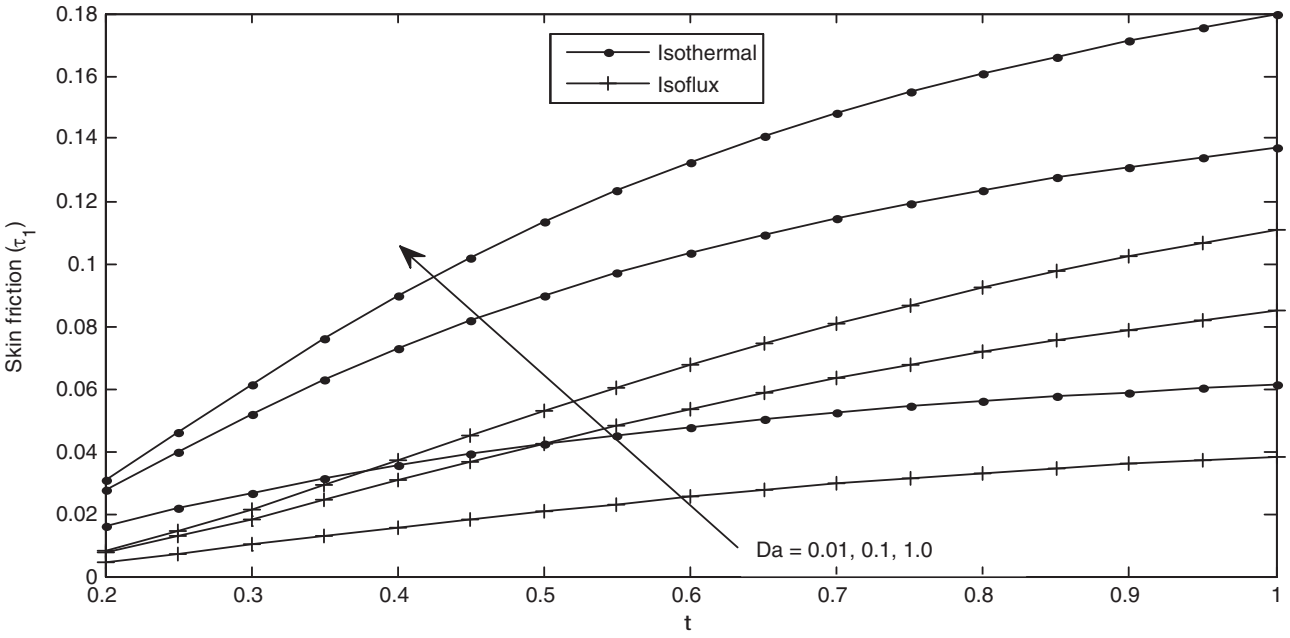

Fig. 8. Skin friction at the outer surface of the inner cylinder versus t for different values of *Da* ($\Gamma = 1.5, Pr = 0.71, \lambda = 2$).

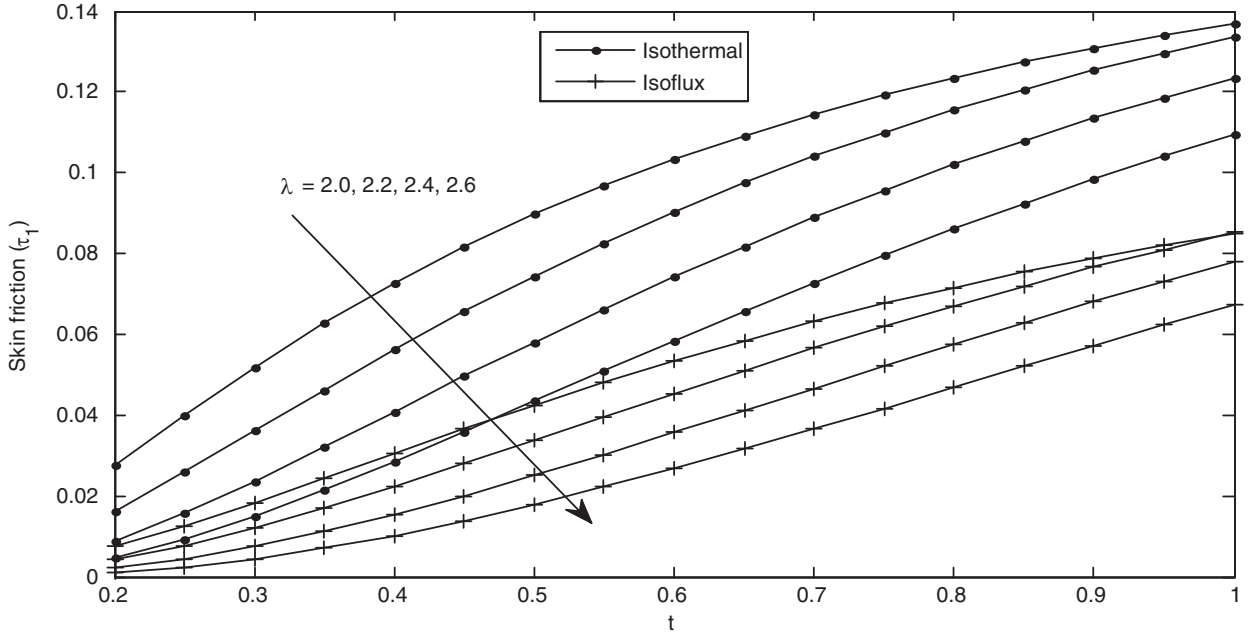

Fig. 9. Skin friction at the outer surface of the inner cylinder versus t for different values of λ ($Da = 0.1, \Gamma = 1.5, Pr = 0.71$).

$$\bar{Q} = 2\pi \int_1^{\lambda} R\bar{U} dR$$
$$= \frac{C_3}{\delta}[\lambda I_1(\lambda\delta) - I_1(\delta)] - \frac{C_4}{\delta}[\lambda K_1(\lambda\delta) - K_1(\delta)] - C_5 \quad (18)$$

where C_1 to C_5 are defined in Appendix.

The solutions (14), (16)–(18) are then inverted to time domain by applying the Riemann-sum approximation stated in Eq. (15).

2.2. Validation of the method

In order to validate the accuracy of the Riemann-sum approximation used in inverting Eqs. (13), (14), (16)–(18), we proceeded to find the solution of the steady-state velocity analytically which is expected to coincide with the transient solution at large time. This is obtained by taking $\frac{\partial()}{\partial t} = 0$ in Eqs. (1) and (2) which in dimensionless form reduces to the following ordinary differential equations Jha [2].

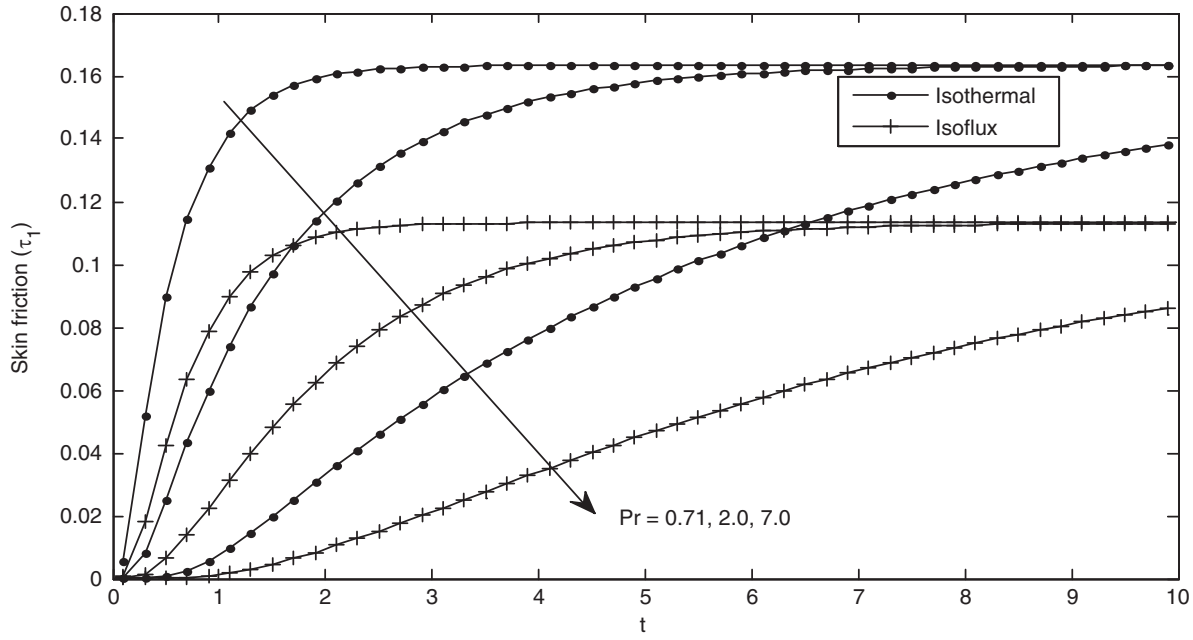

Fig. 10. Skin friction at the outer surface of the inner cylinder versus t for different values of *Pr* (Da = 0.1, Γ = 1.5, λ = 2).

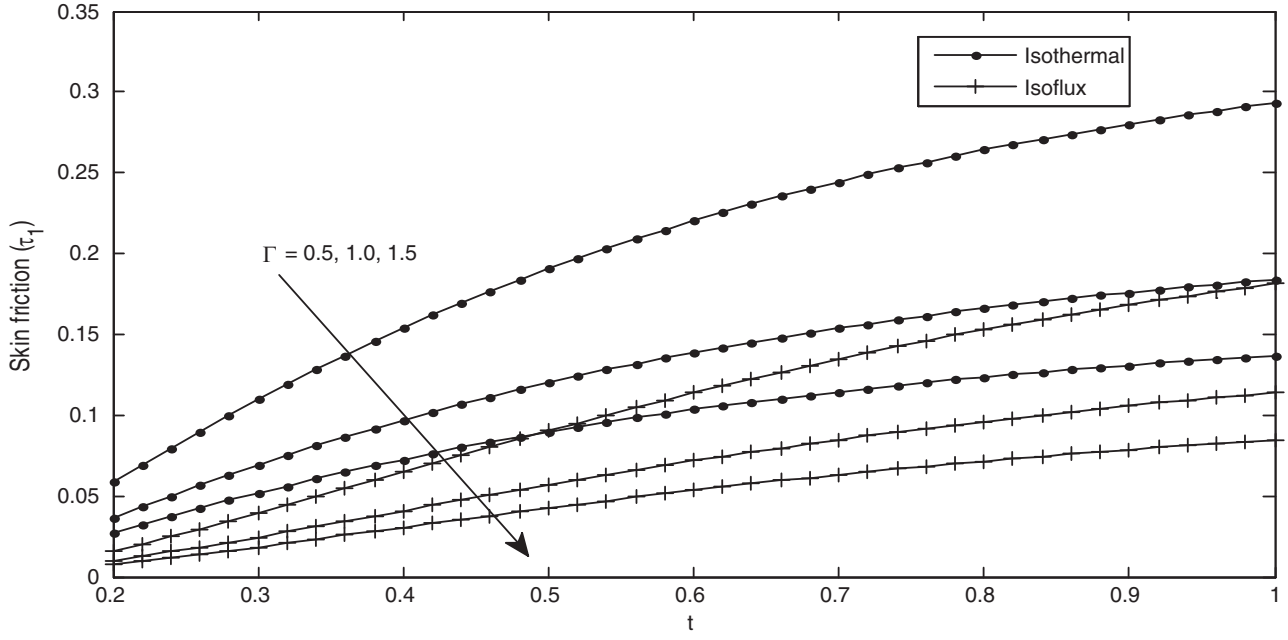

Fig. 11. Skin friction at the outer surface of the inner cylinder versus t for different values of Γ (Da = 0.1, *Pr* = 0.71, λ = 2).

$$\Gamma\left[\frac{d^2U}{dR^2}+\frac{1}{R}\frac{dU}{dR}\right]-\frac{U}{Da}+\theta=0 \tag{19}$$

$$\frac{d^2\theta}{dR^2}+\frac{1}{R}\frac{d\theta}{dR}=0 \tag{20}$$

With the boundary conditions

$$U=0 \quad \frac{d\theta}{dR}=-1 \quad \text{or} \quad \theta=1 \quad \text{at} \quad R=1 \tag{21}$$

$$U=0 \quad \theta=0 \quad \text{at} \quad R=\lambda \tag{22}$$

The set of Eqs. (19)–(22) which is the steady state momentum and energy equation of the present problem under consideration, corresponds with the work of Jha [2]. The numerical values obtained using Riemann-sum approximation for the velocity at large time and Jha [2] is presented in Tables 1 and 2.

To further establish the accuracy of the Riemann-sum approximation approach, the implicit finite difference is used to solve Eqs. (5) and (6) with the initial and boundary condition (7). The numerical values for steady state velocity using the implicit

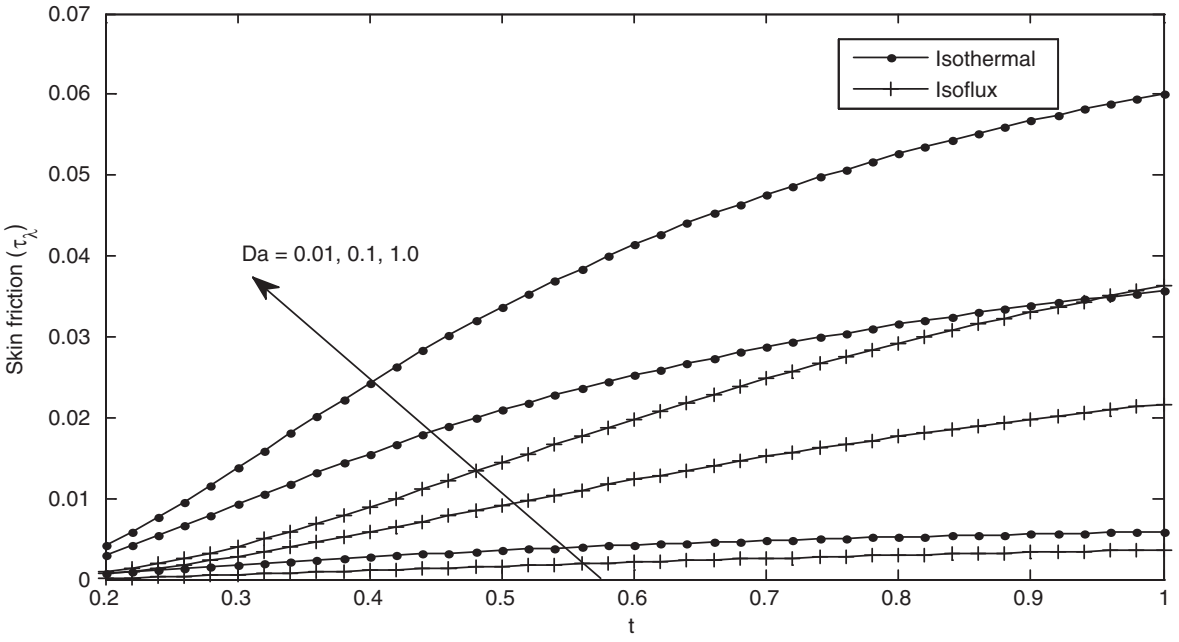

Fig. 12. Skin friction at the inner surface of the outer cylinder versus t for different values of *Da* ($\Gamma = 1.5, Pr = 0.71, \lambda = 2$).

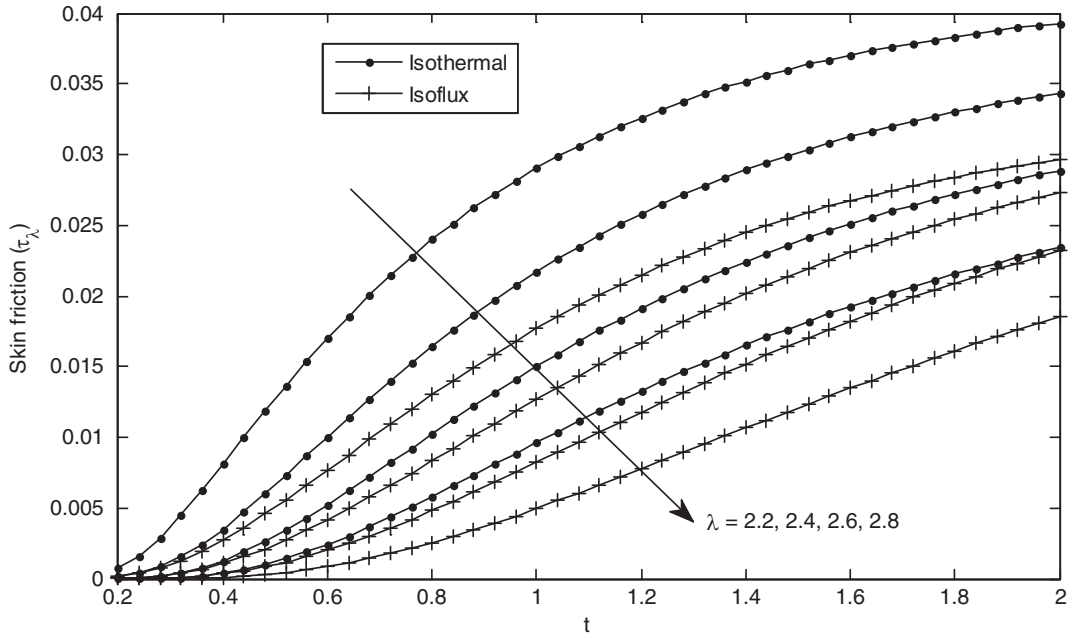

Fig. 13. Skin friction at the inner surface of the outer cylinder versus t for different values of λ ($\Gamma = 1.5, \mathrm{Da} = 0.1, Pr = 0.71$).

finite difference method agrees with the values obtained using Riemann-sum approximation method at large time (See Table 1). It is good to note that, in addition to establishing accuracy at steady state, the numerical values obtained using the implicit finite difference method at transient state also corresponds with the ones obtained using the Riemann-sum approximation approach for small values of time. (See Table 2). Tables 3–5 is also presented to further buttress the accuracy by comparing the steady-state skin friction for different values of λ and *Da*.

3. Results and discussion

In order to get a physical insight into the problem, quantities such as velocity, temperature, skin-friction and mass flow rate have been computed by assigning values of the various controlling parameters and the results are graphically shown in Figs. 2–19.

Figs. 2 and 3 depict the temperature profiles for isothermal and isoflux heating of the outer surface of the inner cylinder for different values of time (t) and (Pr) respectively. From Fig. 2, we

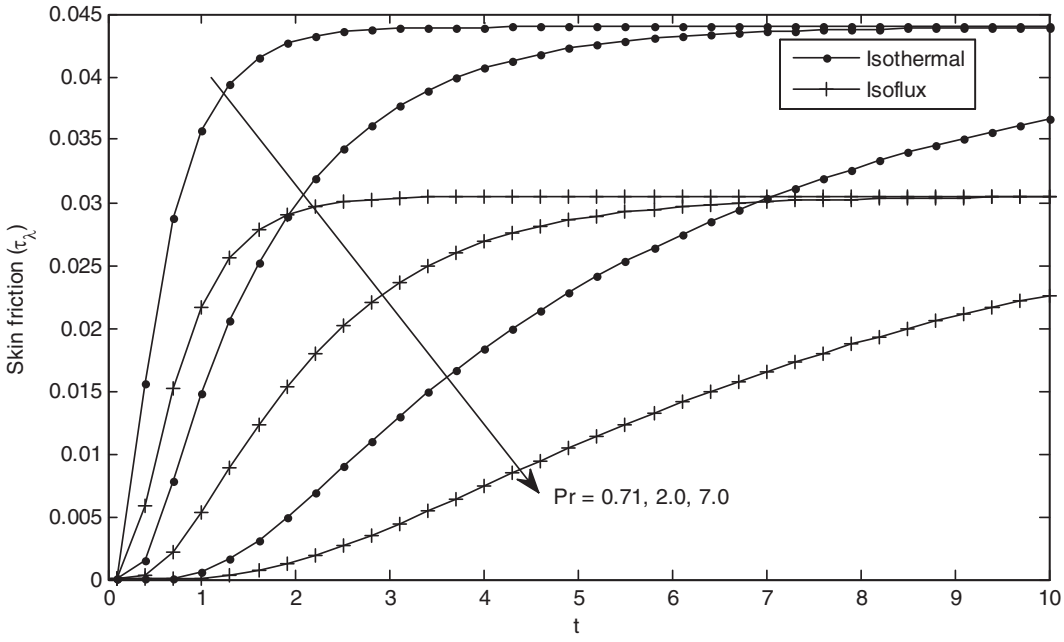

Fig. 14. Skin friction at the inner surface of the outer cylinder versus t for different values of *Pr* (Da $= 0.1, \Gamma = 1.5, \lambda = 2$).

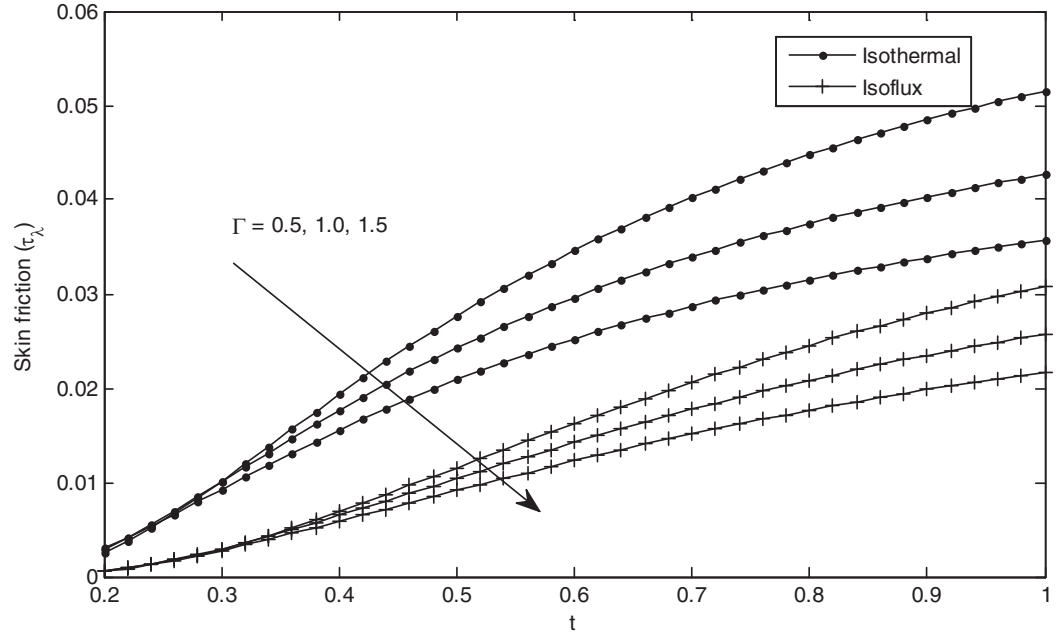

Fig. 15. Skin friction at the inner surface of the outer cylinder versus t for different values of Γ(Da $= 0.1, Pr = 0.71, \lambda = 2$).

observed that the temperature increases with increase in time (t) and finally attains its steady state for both isothermal and isoflux heating at the outer surface of the inner cylinder.

Fig. 3 shows temperature variation with Prandtl number for isothermal as well as isoflux heating at the outer surface of the inner cylinder. It is clear from this figure that temperature decreases with increase in Prandtl number (Pr). This effect can be explained from the fact that as Prandtl number increases, the conduction is less effective in the fluid and the thermal transient is slower.

Figs. 4–7 describes velocity variation for isothermal as well as isoflux heating for different values of t, Da *and* Γ. These figures also show effect of annular gap when it is less or equal to the radius of the inner cylinder or when the annular gap is greater than the radius of the inner cylinder.

Fig. 4 reveals that the velocity increases with increase in time (t) and finally attains its steady state value. It is also clear from the figure that velocity is higher in the case of isothermal heating when the annular gap is less than or equals the radius of the inner cylinder. The reverse trend is observed when the annular gap is greater than the radius of inner cylinder (see Fig. 5).

The effect of Darcy number as well as annular gap on the velocity is presented in Fig. 6. It is clear that velocity is directly proportional Darcy number and annular gap.

Velocity variation for different values of viscosity ratio (Γ) is presented in Fig. 7. From this figure, we observed that velocity decreases with increase in Γ.

Figs. 8–11 reveal the influence of flow parameter $Da, \lambda, Pr, and \Gamma$ on the skin friction (τ_1) at the outer surface of the inner cylinder when the annular gap between the cylinders is less than or equal

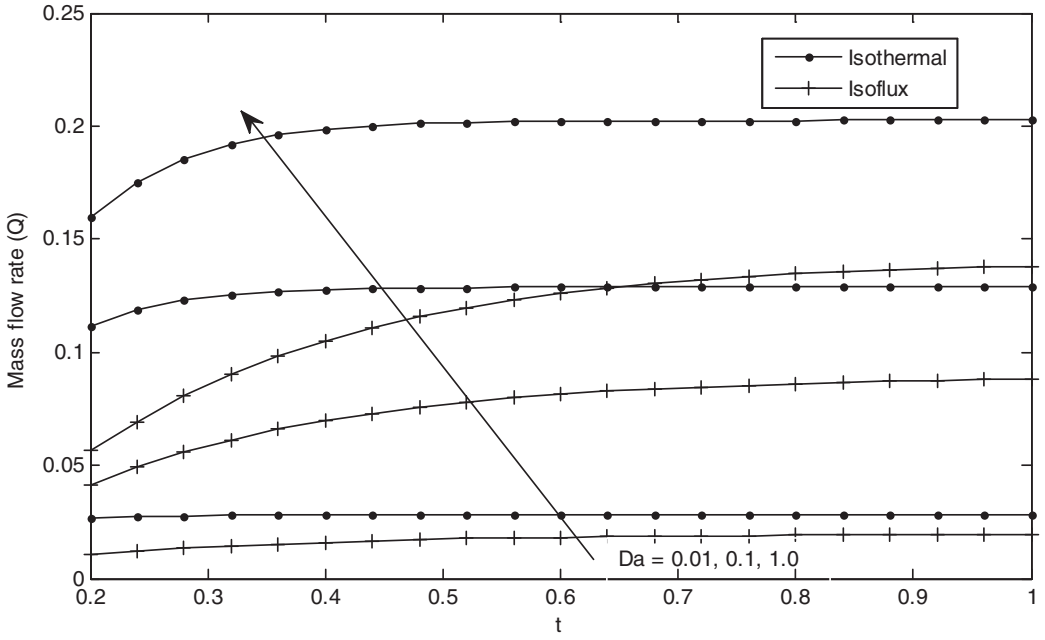

Fig. 16. Distribution of Mass flow rate versus t for different values of Da $(\mathrm{Pr} = 0.71, \Gamma = 1.5, \lambda = 2)$.

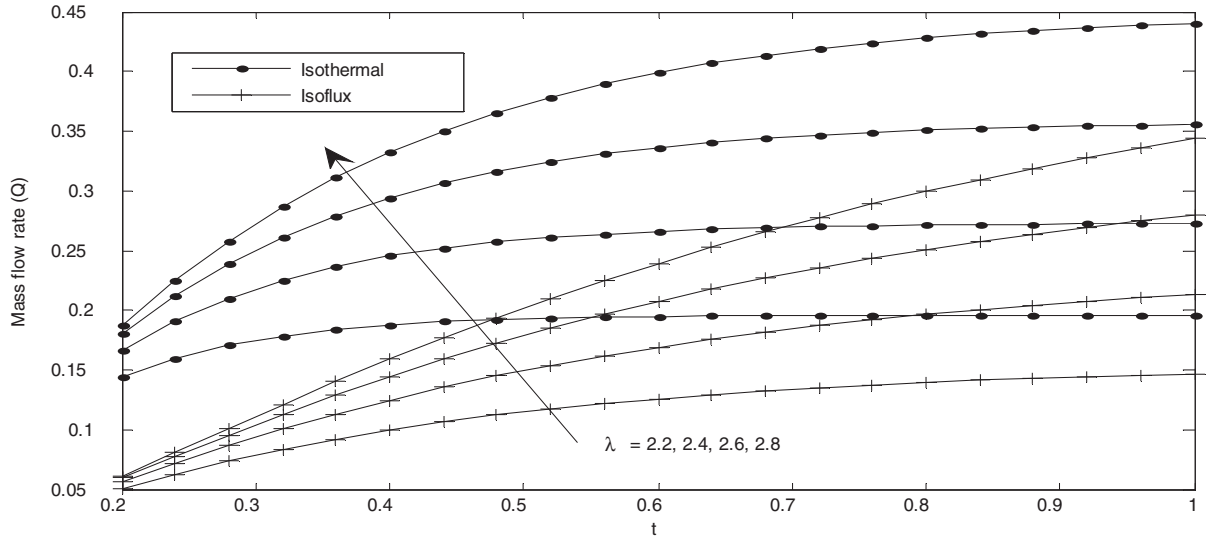

Fig. 17. Distribution of Mass flow rate versus t for different values of λ $(\Gamma = 0.71, \mathrm{Da} = 0.1, Pr = 0.71)$.

to the radius of the inner cylinder for both isothermal and constant heat flux heating of the outer surface of the inner cylinder. It is observed from Fig. 8 that the skin friction (τ_1) increases with time (t) and Darcy number (Da) for a fixed value of λ. In addition, the skin friction is higher for isothermal heating in comparison to isoflux heating.

Variation of skin friction (τ_1) with time (t) and annular gap (λ) at the outer surface of the inner cylinder is shown in Fig. 9 for both isothermal and isoflux heating of the outer surface of the inner cylinder. The skin friction is observed to be an increasing function of time (t) while decreasing function of annular gap (λ). This indicates that by varying the gap between the cylinders or by applying the suitable process of heating, it is possible to control the skin friction at the outer surface of the inner cylinder.

Figs. 10 and 11 present skin friction variation at the outer surface of the inner cylinder for different values of *Pr* and Γ respectively. It is observed that skin friction increases with *Pr* and Γ for both isothermal and isoflux heating. In addition, skin friction attains its steady state faster for smaller values of *Pr* (see Fig. 10).

Fig. 12 shows the skin friction variation at the inner surface of the outer cylinder for different values of time (t) and Darcy number (Da) . This figure reveals that skin friction (τ_λ) increases with *t* and *Da*. Also, the figure further show that the skin friction (τ_λ) is higher when the inner cylinder is isothermally heated in comparison to isoflux heating.

Figs. 13–15 illustrate the skin friction variation (τ_λ) at the inner surface of the outer cylinder for different values of λ, Pr *and* Γ respectively, for isothermal and constant heat flux heating. From these figures, it is evident that the skin friction (τ_λ) decreases with increase in each of the flow parameters λ, Pr *and* Γ. These figures also shows that skin friction increases with time and approaches its steady state status.

Variation of mass flow rate for isothermal and isoflux heating of the outer surface of inner cylinder for different values of Darcy

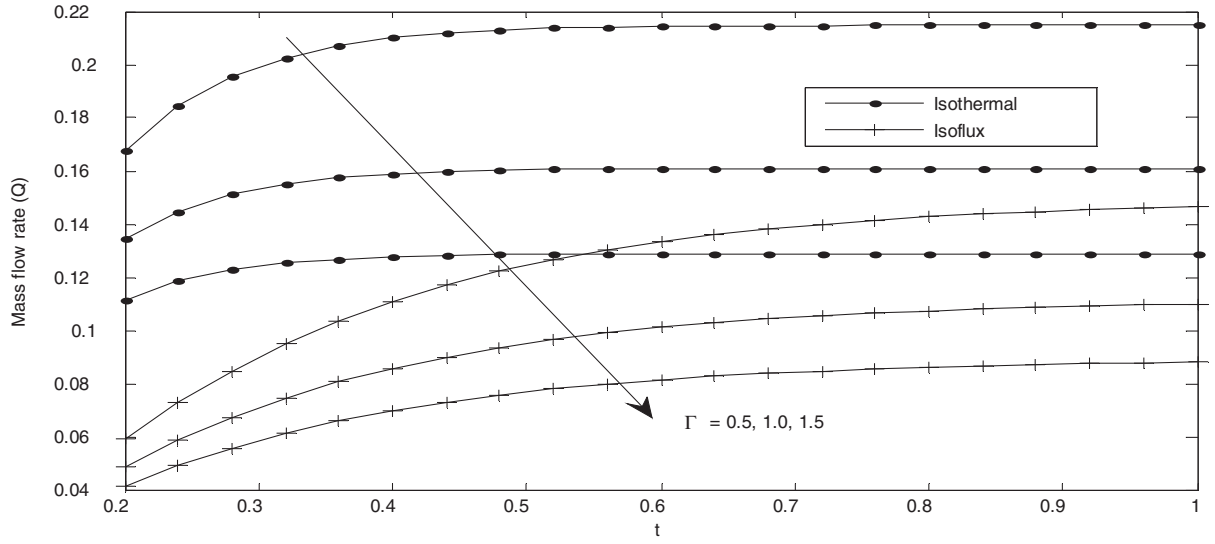

Fig. 18. Distribution of Mass flow rate versus t for different values of Γ (Pr = 0.71, Da = 0.1, $\lambda = 2$).

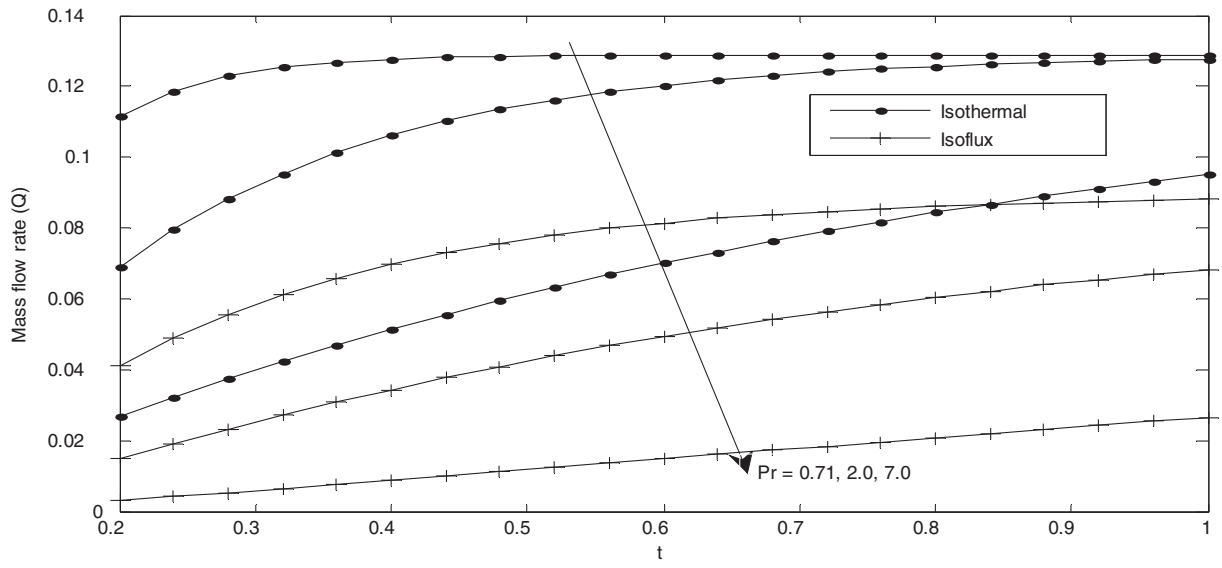

Fig. 19. Distribution of Mass flow rate versus t for different values of *Pr* (Γ = 0.71, Da = 0.1, $\lambda = 2$).

number (Da) and time (t) is presented in Fig. 16. From this figure, mass flow rate is observed to be an increasing function of Darcy number (Da). This is due to the fact that as Da increases, porous medium become more permeable for fluid flow, this in turn enhance the mass flow rate in the annulus. Also mass flow rate increases with time (t) and finally attain its steady state value.

The impact of annular gap (λ) and time (t) on mass flow rate is presented in Fig. 17. It is clear that increase in annular gap enhance the mass flow rate in the annulus.

Figs. 18 and 19 display the variation of mass flow rate for isothermal and isoflux heating at the outer surface of the inner cylinder for different values of Γ *and Pr* respectively for fixed value of annular gap. These figures show that mass flow rate is inversely proportional to Γ *and* Pr.

4. Conclusion

A semi-analytical solution of the mathematical model responsible for transient free-convective flow in an annular porous medium has been obtained in terms of modified Bessel's function. The important outcome of the numerical calculations of the semi-analytical solution is that the transient natural convection flow formation inside the vertical annulus filled with isotropic porous material and saturated with the same fluid can be controlled by applying a suitable phenomenon of heating process and also by varying the gap between the cylinders.

Appendix

$$C_1 = \frac{CK_0(\lambda\sqrt{sPr})}{s[E_1 + I_0(\lambda\sqrt{sPr})\{A\sqrt{sPr}K_1(\sqrt{sPr}) - BK_0(\sqrt{sPr})\}]}$$

$$C_2 = \frac{CI_0(\lambda\sqrt{sPr})}{s[I_0(\lambda\sqrt{sPr})\{BK_0(\sqrt{sPr}) - A\sqrt{sPr}K_1(\sqrt{sPr})\} - E_1]}$$

$$C_3 = \frac{[C_1I_0(\sqrt{sPr}) + C_2K_0(\sqrt{sPr})]K_0(\lambda\delta)}{I_0(\delta)K_0(\lambda\delta) - I_0(\lambda\delta)K_0(\delta)}$$

$$C_4 = \frac{[C_1I_0(\sqrt{sPr}) + C_2K_0(\sqrt{sPr})]I_0(\lambda\delta)}{I_0(\lambda\delta)K_0(\delta) - I_0(\delta)K_0(\lambda\delta)}$$

$$C_5 = \frac{[C_1\{\lambda I_1(\lambda\sqrt{sPr}) - I_1(\sqrt{sPr})\} - C_2\{\lambda K_1(\lambda\sqrt{sPr}) - K_1(\sqrt{sPr})\}]}{\left[\Gamma sPr - \left(\frac{1}{Da} + s\right)\right]}$$

$$E_1 = K_0(\lambda\sqrt{sPr})[A\sqrt{sPr}I_1(\sqrt{sPr}) - BI_0(\sqrt{sPr})]$$

References

[1] V. Vafai, C.L. Tien, Boundary and inertia effects on flow and heat transfer in porous media, Int. J. Heat Mass Transfer 24 (1981) 195–204.
[2] B.K. Jha, Free-convection flow through an annular porous medium, Heat Mass Transfer 41 (2005) 675–679.
[3] T. Paul, A.K. Singh, Natural convection between coaxial vertical cylinders partially filled with a porous material, Forschug Im ingenieurwesen 64 (6) (1998) 157–162.
[4] H.M. Joshi, Fully developed natural convection in an isothermal vertical annular, Int. Commun. Heat Mass Transfer 14 (1987) 657–664.
[5] R.K. Singh, A.K. Singh, Effect of induced magnetic field on natural convection in vertical concentric annuli, Acta. Mech. Sin. 28 (2) (2012) 315–323.
[6] B.K. Jha, S.B. Joseph, A.O. Ajibade, Transient free-convective flow through a vertical porous annulus, Eng. Part E. J. Process Mech. Eng. 225 (2012) 1989–1996.
[7] K. Javaherdeh, M.M. Nejad, M. Moslemi, Natural convection heat and mass transfer in MHD fluid flow past a moving vertical plate with variable surface temperature and concentration in a porous medium, Eng. Sci. Technol. Int. J. 18 (2015) 423–431.
[8] B.K. Jha, J.O. Odengle, Unsteady MHD Couette flow in composite channel partially filled with porous material: a semi-analytical approach, Transp. Porous Media 107 (2015) 219–234.
[9] A. Vanita Kumar, Effect of radial magnetic field on natural convection flow in alternate conducting vertical concentric annuli with ramped temperature, Eng. Sci. Technol. Int. J. 19 (3) (2016) 1436–1451.
[10] F. Arpino, G. Cortellessa, A. Mauro, Transient thermal analysis of natural convection in porous and partially porous cavities, Numer. Heat Transfer, Part A 67 (2015) 605–631.
[11] N. Massarotti, M. Ciccolella, G. Cortellessa, A. Mauro, New benchmark solutions for transient natural convection in partially porous annuli, Int. J. Numer. Methods Heat Fluid Flow (2016), http://dx.doi.org/10.1108/HFF-11-2015-0464.
[12] M. Khan, E. Naheed, C. Fetecau, T. Hayat, Exact solutions of starting flows for second grade fluid in a porous medium, Int. J. Nonlinear Mech. 43 (2008) 868–879.
[13] M. Khan, M. Saleem, C. Fetecau, T. Hayat, Transient oscillatory and constantly accelerated non-Newtonian flow in a porous medium, Int. J. Nonlinear Mech. 42 (2007) 1224–1239.
[14] T. Paul, B.K. Jha, A.K. Singh, Free convection between vertical walls partially filled with porous medium, Heat Mass Transfer 33 (1998) 515–519.
[15] C. Beckemann, R. Vistkanta, S. Ramdhyani, A numerical steady of non-darcian natural convection in a vertical enclosure filled with a porous medium, Numerical Heat Transfer 10 (1986) 557–570.
[16] A. Khalid, I. Khan, A. Khan, S. Shafie, Unsteady MHD free convection flow of Casson fluid past over an oscillating vertical plate embedded in a porous medium, Eng. Sci. Technol. Int. J. 18 (2015) 309–317.
[17] F. Arpino, G. Cortellessa, M. Dell'Isola, N. Massarotti, A. Mauro, High order explicit solutions for the transient natural convection of incompressible fluids in tall cavities, Numer. Heat Transfer Part A: Appl. An Int. J. Comput. Method 66 (2014) 839–862.
[18] B.K. Jha, B. Aina, Magnetohydrodynamic natural convection flow in a vertical micro-porous-annulus in the presence of radial magnetic field, J. Nanofluids 5 (2016) 1–10.
[19] D.Y. Tzou, Macro to Microscale Heat Transfer: The Lagging Behavior, Taylor and Francis, London, 1997.